Species measurements in the beam of an ionic liquid ferrofluid electrospray source

Kurt J. Terhune[*] and Lyon B. King[†]
Michigan Technological University, Houghton, MI, 49931, USA

Michael L. Hause[‡] and Benjamin D. Prince[§]
Air Force Research Laboratory, Kirtland AFB

Nirmesh Jain[**] and Brian S. Hawkett[††]
The University of Sydney, NSW 2006, Australia

An ionic liquid ferrofluid (ILFF) using 1-ethyl-3-methylimidazolium bis(trifluoromethylsulfonyl)imide (EMIM-NTf2) as the carrier liquid was emitted from the peak formed via the Rosensweig instability and the electrospray beam was measured using quadrupole and TOF mass spectrometry. The Rosensweig instability peak source (RIPS) was found to operate in three stable emission current modes: transient-emission, low-current, and high-current. Both quadrupole and linear TOF mass spectra for the final two modes were collected, and revealed that the charged-particle species within the electrospray beam varied between the two emission current modes. No correlation between the magnetic field strength and the collected mass spectra was measured. Mass flow measurements using a quartz crystal microbalance revealed that the RIPS only operated at a high mass flow rate of 3-5 ng/s during the startup transient-emission mode and otherwise ran at mass flow rates of 0.03-0.3 ng/s indicating the absence of droplet species during the majority of emission. The RIPS quadrupole mass spectra were compared to a pure ionic liquid needle source quadrupole spectra and it was discovered that multiple species exist in the ILFF electrospray that are attributed to fragments respective ion species, with some species partially comprised of fragments from the polymer used for steric stabilization of the nanoparticles; specifically the block that comprises the stabilization group, poly(N,N-dimethylacrylamide), and the end functionalizing group, CH3CHCOOH.

Nomenclature

B	=	magnetic field
d	=	extraction distance
E	=	electric field
g	=	gravitational constant
γ	=	liquid surface tension
H	=	magnetic field strength
I	=	electrical current
I_{sp}	=	specific impulse
L_{TOF}	=	length of TOF chamber
λ_c	=	critical wavelength of the Rosensweig instability
m	=	mass
M	=	magnetization
P	=	power

* Graduate Research Assistant, Mechanical Engineering, 815 RL Smith Building, AIAA Student Member.
† Professor, Mechanical Engineering, 1014 RL Smith Building. AIAA member.
‡ Research Chemist, Boston College Institute for Scientific Research, Space Vehicles Directorate, 3550 Aberdeen Ave SE, Building 570.
§ Research Chemist, Space Vehicles Directorate, 3550 Aberdeen Ave SE, Building 570. AIAA Member
** Research Associate, School of Chemistry and Key Centre for Polymers and Colloids, Chemistry F11
†† Associate Professor, School of Chemistry and Key Centre for Polymers and Colloids, Chemistry F11

q = electrical charge
r = radius of Taylor cone apex
ρ = liquid density
σ_B = magnetostatic stress
σ_E = electrostatic stress
σ_γ = surface tension stress
t_{flight} = time-of-flight
T = Thrust
u_e = exit velocity
u_i = particle velocity
U_i = TOF repeller voltage
U_0 = extractor voltage
V = volume

I. Introduction

MONODOMAIN magnetic nanoparticles suspended in a carrier liquid produce a colloid that is susceptible to electromagnetic fields. The nanoparticles are coated in a polymer surfactant to prevent agglomeration, and are of such small diameter that Brownian motion inhibits sedimentation of the particles.[1] Because of their unique magnetic, rheological, and thermal properties ferrofluids are exploited for multiple applications, specifically as a damping agent in audio speakers,[2,3] as a medium for heat transfer and lubrication in bearings,[1,3] and for biomedical drug delivery,[4,5] hyperthermia[4,6], *in vitro* applications,[4] and within MRI machines.[4,5] More recently ferrofluids were proposed as propellant for electrospray space propulsion devices.[7,8]

When a ferrofluid is subjected to a strong magnetic field, the domains of the individual particles align with the field lines. Furthermore, perturbations on the surface of the fluid cause localized concentrations of the magnetic field. The magnetic fluid is attracted to the higher concentrations of magnetic field and an instability forms which causes the fluid to bulge at these locations. This instability, known as the Rosensweig instability, is balanced by the surface tension of the ferrofluid, which pulls against the change in the liquid surface.[1,9] The result of this force balance is an arrangement of static fluid peaks, seen in Figure 1. If the carrier liquid of the ferrofluid is stable in vacuum environments, such as an ionic liquid (IL), these static peaks become attractive for space propulsion.

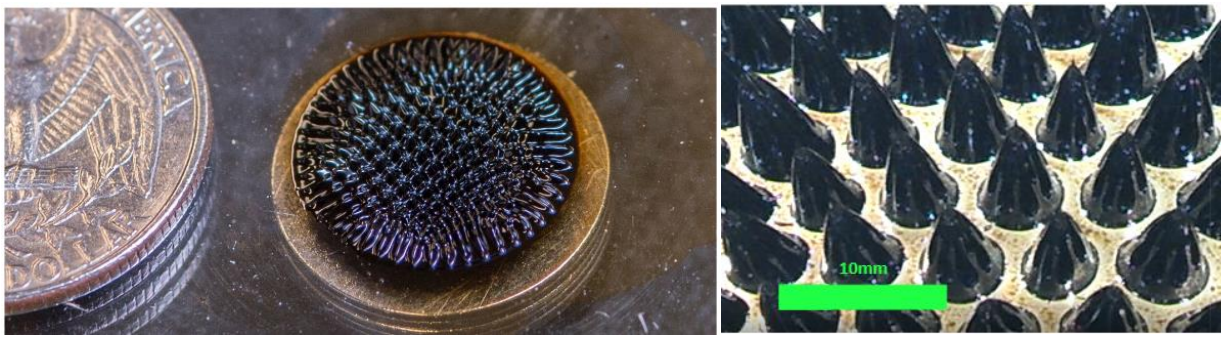

(a) **(b)**

Figure 1. Images of the Rosenweig instability in a FerroTec EFH-1 ferrofluid. [7]

Ionic liquid ferrofluid (ILFF) electrosprays operate by applying an electric field to the static peaks formed by the Rosensweig instability. The electric field produces a stress on the ILFF peaks which pulls at their surface and reduces the radius of each tip. The electrostatic stress is countered by liquid surface tension, which resists any change to the surface of the liquid. The electric field is consequently enhanced by the reduced radius of the Rosensweig peak, and in-turn further reduces the tip radius of the peak until it overcomes the surface tension balance. For sufficiently strong electric fields the result is a Taylor cone-jet and an electrospray beam.[7,8] A schematic of this phenomenon is provided in Figure 2.

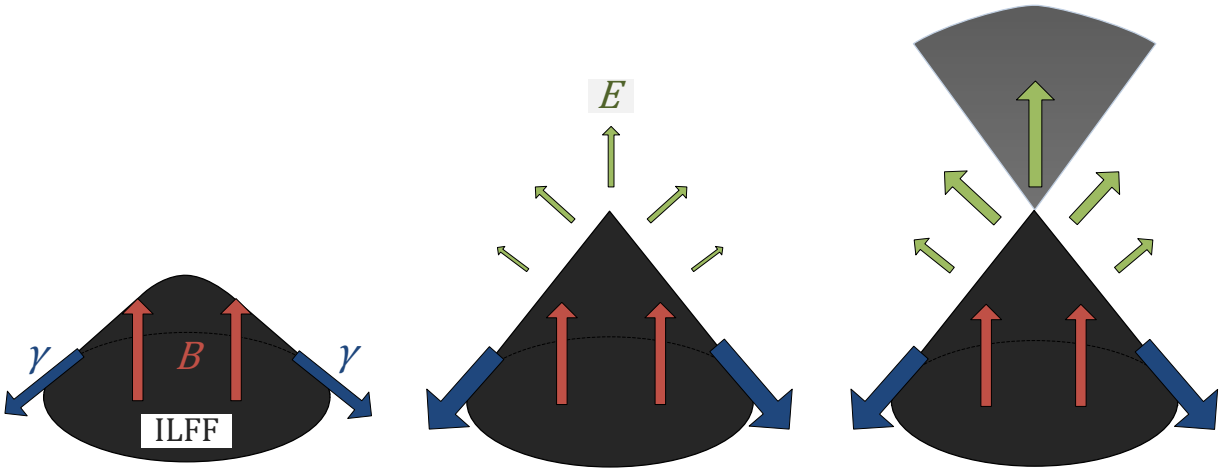

Figure 2. Schematic demonstrating electrospray emission from a Rosensweig instability peak. In (a) a magnetic field, B, is applied and balanced by surface tension, γ. In (b) electric, E, and magnetic fields are applied and balanced by surface tension. In (c) the electric and magnetic fields overcome surface tension and electrospray onset occurs.

II. Goal of Study

Within electrostatic propulsion devices, such as electrospray beams, compromise must always be made between the thrust-to-power ratio of the thruster (Equation 1) and its specific impulse, I_{sp} (Equation 2). Either a thruster can complete a mission using higher thrust-to-power, which cuts down on mission time but requires more propellant, or using higher I_{sp}, which uses the propellant more efficiently, but requires a longer mission time. The dependent variable in both missions, which creates this necessary compromise, is the mass-to-charge ratio (m/q) of the emitted beam, as shown in Equations 1 and 2.

$$T/P = \sqrt{\frac{2}{U_0}\frac{m}{q}} \tag{1}$$

$$I_{sp} = \sqrt{2U_0\frac{q}{m}} \tag{2}$$

Therefore, to properly match an electrospray thruster to a specific mission, the m/q of the electrospray beam must be measured and understood. For pure IL electrosprays, this measurement is typically accomplished through mass spectrometry, and mass spectra for those ILs used in thrusters have been studied extensively.[10-15] However, no studies have been conducted to collect the mass composition of a beam from an ILFF electrospray source, which operates using a new fluid and additional field, providing motivation to conduct the research described in this paper.

One goal of this study is to determine the mass-to-charge composition of an ILFF electrospray beam emitted from a single Rosensweig instability peak. Specifically, the relative mass-to-charge composition of the electrospray beam will be measured while the peak undergoes adjustments in emission current and magnetic field strength. A second goal is to compare ILFF electrospray mass spectra to spectra from a solid needle emitter to define the differences between the two sources. Quantifying the ion species and particles that are emitted from the Rosensweig instability peak and directly comparing them to those from a needle emitter will provide a basis in determining their relevance in space propulsion.

III. Background

A. Ferrofluids

The nanoparticles of a ferrofluid maintain their colloidal nature through their small size and a surfactant coating. There are several types of surfactants that have been used to accomplish this feat,[16-18] each chosen based on its affinity for the surface of the particles and its solubility in the carrier liquid. Several examples of polar groups that can have affinity for magnetic particle surfaces are carboxyl, phosphate, phosphoric acid, and sulfosuccinate.[18] Jain et al. [16] used a short chain block copolymer surfactant wherein one block anchors the surfactant to the surface of the particles while the other block, which is highly soluble in the continuous phase, provides steric stabilization. To stabilize the magnetic particles in the ionic liquid EMIM-NTf_2, the block copolymer 10MAEP-60DMAM was used (Figure 3). The polymer molecule is comprised of 10 poly(monoacryloxyethyl phosphate) (PMP) blocks, 60 poly(N,N-dimethylacrylamide) (PDA) blocks, a RAFT end group ($CS_3C_4H_9$) and a functionalizing group ($CH_3CHCOOH$). The 60 PDA blocks and the functionalizing group that comprise the right half of the polymer molecule in Figure 3 are referred to as the stabilization block and extend into the IL to provide steric stabilization.

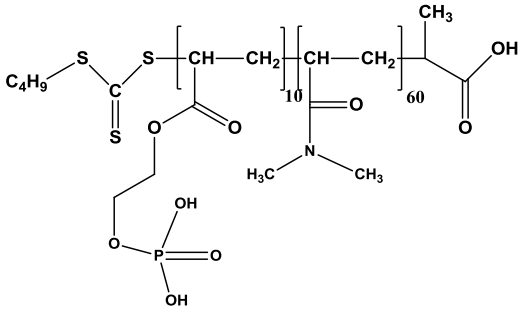

Figure 3. Schematic of the block copolymer used to stabilize maghemite particles in the ionic liquid EMIM-NTf_2.

B. Ionic Liquid Ferrofluid Electrosprays

The first ferrofluid that used an ionic liquid as the carrier liquid was produced by Jain, et al. in 2011.[17] These ILFFs used ethylammonium nitrate (EAN) and 1-ethyl-3-methylimidazolium acetate (EMIMAc) and 1-ethyl-3-methylimidazolium thiocyanate (EMIM-SCN). Though suitable for peak formation via the Rosensweig instability, these ILs were less-suitable for electrospray due to their relatively high vapor pressures and viscosities.[7,8] A collaboration between Jain and Hawkett, and Meyer and King led to an ILFF using EMIM-NTf_2 as the carrier liquid;[8] EMIM-NTf_2 is less viscous than EAN, has near zero vapor pressure, and has extensive use in the electrospray arena.

Research on the electrospray of ferrofluids includes emission experiments to demonstrate the ILFF electrospray technology,[7,8] and wavelength measurement experiments of non-conducting oil-based ferrofluids to determine the peak density as a function of the $B\nabla B$ fields.[8]

C. Mass Spectrometry of Ionic Liquid Electrosprays

Mass spectrometry is an established method of analyzing electrospray thrusters to determine their performance as space propulsion devices.[10-15,19-26] Mass spectrometers can measure the m/q values of the emitted ion and droplet species. As previously stated, understanding the different ion and droplet species within the emitted beam indicate whether the thruster can be used on a high thrust or high I_{sp} mission; some thrusters can operate in variable modes giving them the ability to complete both types of missions.

Within the extensive literature on IL electrospray sources, mass spectrometry provided a means to differentiate between two general types of sources, needle and capillary. Examples of mass spectra of electrosprays from both sources using the IL 1-butyl-3-methylimidazolium dicyanamide (BMIM-DCA) are shown in Figure 4.[20,21] From these two spectra an important distinction is seen; the needle source produces only the two, possibly three, lightest ion species while the capillary source emits greater than four ion species. With regard to the thrust-to-power vs. I_{sp} compromise, this implies that the needle operates with lighter masses, higher I_{sp}, and lower thrust, whereas the capillary operates with larger masses, more thrust, but lower I_{sp}.

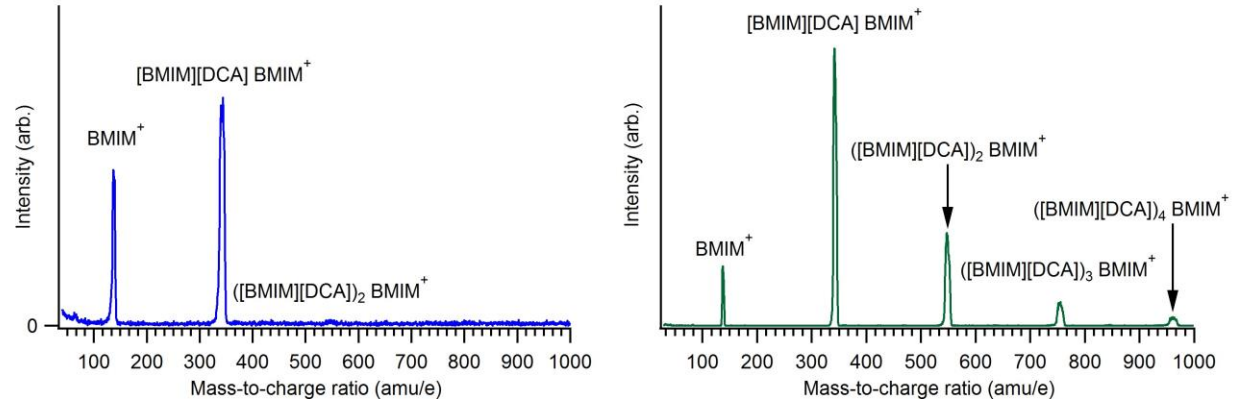

Figure 4. Mass spectra of an BMIM-DCA electrospray beam from (a) a needle source[20] and (b) a 50 um tip diameter capillary source with a flow rate of 0.3 nL/s at 15 degrees off the beam axis.[21]

The Rosensweig instability peak source (RIPS) is another type of fluid meniscus drastically different from both solid needles and hollow capillaries, as illustrated in Figure 2. And, as Figure 4 illustrates, electrospray sources do not necessarily operate in the same manner. Therefore, mass spectra of the ILFF electrospray from a RIPS must be measured to determine its similarities to and differences from needle and capillary sources and to define its relevance to the electrostatic propulsion arena.

D. Time-of-flight Mass Spectrometry

Time-of-flight (TOF) mass spectrometers are based on the charged particles and droplets extracted from a source using a constant potential having a unique velocity proportional to each particle's m/q. To separate the particles based on this ratio, the TOF mass spectrometer pulses an extraction electrode to voltage U_i placed perpendicular to the axis of the electrospray beam to capture a volume of the beam and accelerate it toward a charge-exchange multiplier (CEM) or multichannel plate (MCP). Each particle's TOF is defined as the difference between the time at which the extraction plate is pulsed and the time at which the particle is recorded by the CEM or MCP. A particle's TOF can be directly related to its m/q through the relationship between electrical and kinetic energy of the particles, shown in Equation 3.

$$E_i = \frac{m \cdot u_i^2}{2} = q_i U_i \tag{3}$$

Rearranging Equation 3, and substituting the length of the TOF chamber (L_{TOF}) divided by the TOF (t_{flight}) for the velocity, a relationship is derived for the m/q of a species of particles based on the TOF of the particles, Equation 4.

$$\frac{m}{q_i} = 2U_i \left(\frac{t_{flight}}{L_{TOF}}\right)^2 \tag{4}$$

IV. Experimental Methods and Apparatus

Experiments using an ILFF electrospray apparatus and a needle electrospray apparatus were conducted in the quadrupole and TOF facilities at the Air Force Research Laboratory (AFRL) on Kirtland Air Force Base and the ultra-high vacuum facility within the Ion Space Propulsion (Isp) Laboratory at Michigan Technological University. The specifics of the testing facilities and the electrospray apparatuses are described in the sections IV-A and IV-B. The procedures for the experiments are provided in section IV-C.

A. Facilities

i. Time-of-flight Mass Spectrometer Facility

The AFRL houses a TOF mass spectrometer that can detect particles in the range of a couple amu/e to 200,000 amu/e. The facility is a 1-meter long by 0.254-meter wide by 0.254-meter tall reflectron flight-tube detection chamber that is situated orthogonal to a 0.5-meter long source chamber. A multichannel plate (MCP) is used as the detector and is positioned at both ends of the reflectron flight-tube to provide both linear and reflectron TOF measurements. The source chamber is maintained at a pressure of 10^{-7} torr, while the detection chamber is

maintained at approximately 2 x 10^{-8} torr. The pressures are achieved using two 250 l/s turbo-molecular pumps backed by one 600 l/min dry scroll pump.

Also housed in the TOF mass spectrometer are multiple lenses, grids and deflectors, attached at the end of the source (discussed in section IV-C) used to maximize the beam intensity entering the TOF pulsing region. The pulsing region consists of a pair of parallel plates which are parallel to, but offset from, the beam axis. Each plate has a gridded aperture to allow orthogonal transmission of ion species when the voltages on the plates are pulsed. Continuing along the original beam axis, a quartz crystal microbalance (QCM), used to quantify the mass flow rate, and a Faraday cup, used to measure the current of the beam, are located after a 6 mm aperture at the end of the parallel plates. These devices are positioned by means of a linear translation stage allowing rapid switching of the two devices. The QCM provides a measure of the mass flow rate of electrospray by measuring the accumulation of a uniform layer of the condensed beam products on a quartz crystal. The additional layer changes the natural frequency of the crystal which is directly translating to thickness-, or mass accumulation-, per-second. The maximum detectable mass flow rate on the QCM is on the order of 100 ng/s.

ii. Quadrupole Mass Spectrometer Facility

The AFRL also houses a quadrupole mass spectrometer which can detect m/q in the range of 20-1000 amu/e. The facility is a 0.75-meter long by 0.254-meter wide by 0.254-meter tall chamber with an off-axis channeltron detector situated at the end of the quadrupole chamber. Ions are generated in the source chamber using the identical source setup as that used in the TOF apparatus. Ions emitted from the source are focused and introduced through a small aperture separating the source and quadrupole chambers. These ions immediately encounter the quadrupole as they enter the detection chamber and are directed through a three-grid retarding potential analyzer and are then detected by an off-axis channeltron detector. Signal generated in the channeltron is directed into two amplification channels of a Stanford Research Systems SR445A pre-amplifier and the resulting signal is directed to discriminator/counting electronics. Also located in the facility are an RPA for beam energy determination, a Faraday cup for current, and a QCM for mass flow measurements.

iii. Ultra-High Vacuum Facility

The ultra-high vacuum (UHV) facility at Michigan Tech (see Figure 5) is approximately 0.5 meters in diameter and 0.5 meters in length, with a base pressure of 10^{-9} torr. High vacuum pressures are achieved using a 280 l/s turbo-molecular pump with a 110 l/min backing dry scroll pump; ultra-high vacuum pressures are achieved using a 300 l/s combination ion-sublimation pump. Also attached to the facility is a 90x trifocal, stereo microscope with a digital color camera that is used for *in-situ* imaging and video capture.

Other test equipment accessible in this facility include a Matsusada AMT-5B20 high voltage amplifier capable of ±5 kV output at 20 mA, a Tektronix CFG253 signal generator, EEVBlog µCurrent micro-ammeters, and a Keithley 2410 Sourcemeter. The output signals from each piece of test equipment can be recorded through an NI PXI-1033 data acquisition chassis via a SCB-68 connector block.

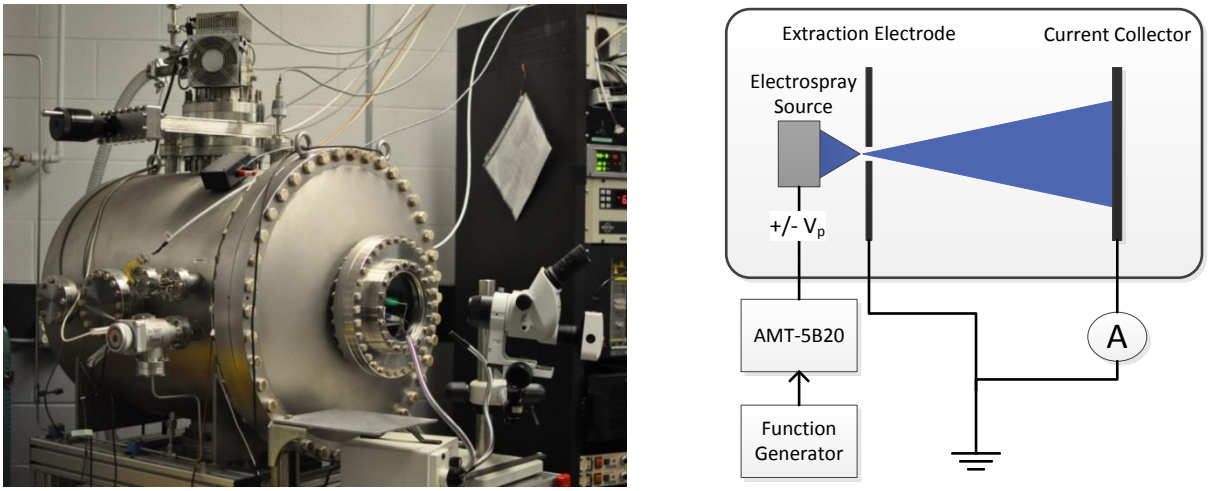

Figure 5. Left: Photograph of ultra-high vacuum facility at Michigan Technological University. Right: Schematic of an ILFF electrospray during current collection while in AC mode.

B. Rosensweig Instability Peak Source Apparatus

The Rosensweig Instability Peak Source (RIPS) apparatus used in the ILFF electrospray experiments is shown in Figure 6. The apparatus is comprised of five main components; the extractor plate, the collector plate, the isolation block, the ILFF reservoir, and the neodymium magnets. The extractor plate is stainless-steel and has a 1-mm aperture. It was offset from the reservoir surface by 3 mm. The collector plate (not shown) was only used in the emission experiments in the UHV facility, and is a stainless-steel plate offset 10 mm from the extractor plate. The isolation block was machined from PTFE and provided isolation between the reservoir, which is biased during testing, and the magnets and the testing chamber.

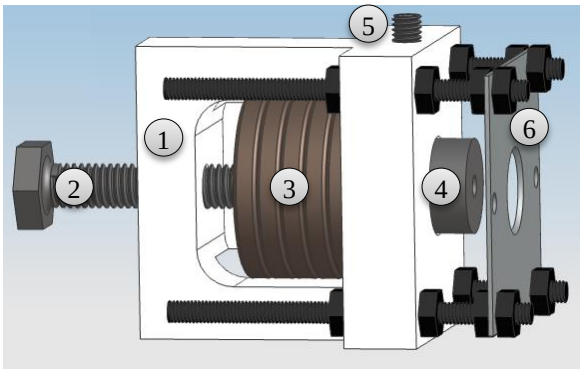

1. PTFE Isolation Block
2. Set Bolt
3. Neodymium Magnets (up to three)
4. SS Reservoir
5. Set Screw/Biasing Element
6. Extraction Plate

Figure 6. Rosensweig electrospray apparatus for TOF facility experiments with components denoted.

The reservoir is an important component of this source as it was required to both hold the ILFF and designed such that a single Rosensweig peak formed. To accomplish this, a 4-mm-deep hole was machined into a SS cylinder to create the reservoir, and the diameter of the reservoir was chosen to be the critical wavelength, λ_c, which was 0.5 mm for this ILFF with an applied magnetic field strength of 520.5 Gauss (Figure 7). The reservoir hole is also chamfered at the top face to reduce boundary effects on the Rosensweig peak.

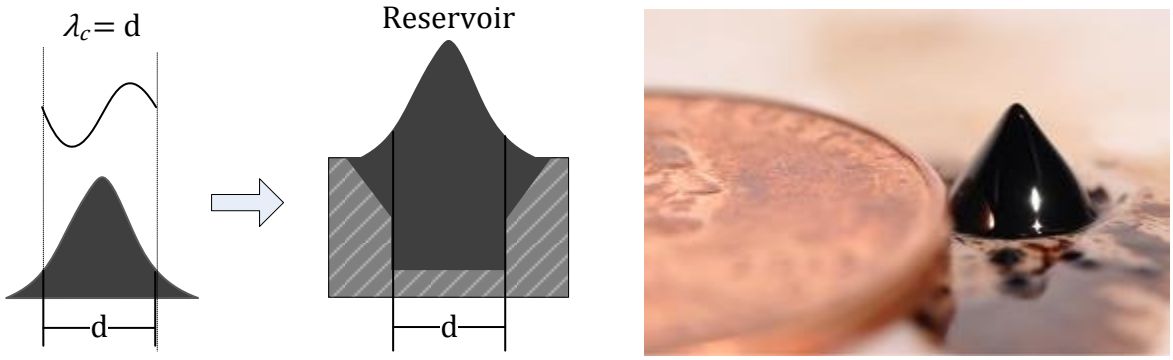

(a) **(b)**

Figure 7. Illustration showing how the design of the ILFF reservoir is defined by the critical wavelength of the Rosensweig instability peak under the magnetic field strength of 520.5 Gauss.

Because the magnetic field is a defining feature of ILFF RIPS it was desired to study the emission at different values of magnetic field intensity. To produce varying magnetic fields strengths one, two, and three 25.4-mm-diameter, N52-grade, neodymium permanent magnets were placed behind the ILFF reservoir, creating field strengths at the reservoir surface (measured with no fluid in the reservoir) of 333.9, 520.5, and 690.4 Gauss, respectively.

C. Experimental Procedures

i. Rosensweig Instability Peak Source Experiments

Emission experiments on the ILFF electrospray from the RIPS apparatus were conducted in the UHV facility at Michigan Tech via the following procedure. The preparation procedure included cleaning all components via sonication in ethanol. After cleaning, the ILFF reservoir was secured in the PTFE block and one, two, or three

permanent magnets were inserted into the block to produce the desired magnetic field strength. Next the ILFF was dispensed into the reservoir via a syringe pump. The ILFF was composed of 27 wt% iron oxide nanoparticles, 4.5 wt% copolymer, and 68.5 wt% EMIM-NTf_2. The volume of ILFF used in each test was held at a constant 20 µL. The extractor plate was placed at approximately 1.5 mm from the apex the Rosensweig instability peak prior to emission and the aperture was centered on the peak axis. The extractor plate was biased using a 0.5 Hz square wave overlaid on a two-minute ramp from ground to the maximum peak voltage and back to ground. The current on the collector plate was recorded during the entire ramp.

Beam TOF spectra of the electrospray from both a conventional externally wetted needle as well as from a Rosensweig instability peak were recorded in these experiments. For the linear TOF experiments using the RIPS the preparation procedure was the same as for the emission experiments in the UHV facility, except the volume of ILFF used was 18 µL. The volume change was necessary for emission of the electrospray from a horizontal position; it did not affect the electrospray from the RIPS. Once the apparatus was assembled, it was attached to a lens stack and then placed into the TOF source chamber. The QCM was placed downstream of the source to acquire start-up mass measurements, after which the Faraday cup was moved into the downstream position.

Emission from the Rosensweig source was accomplished by biasing both the reservoir and the extractor plate with respect to facility ground. A 0.5-Hz square wave with constant amplitude of ±800 V was applied to the reservoir; a second 0.5-Hz square wave with varying peak-to-peak amplitude was applied to the extractor plate. The two square waves were 180 degrees out of phase. Typical starting voltages (difference between needle and extractor potentials) ranged from |2400 V| to |3000 V|, depending on the magnetic field strength applied to the ILFF. The reservoir bias with respect to ground results in the maximum mean kinetic energy of the cations and anions of +800 eV/q and -800 eV/q, respectively, although the kinetic energy can be lower under some circumstances.[21]

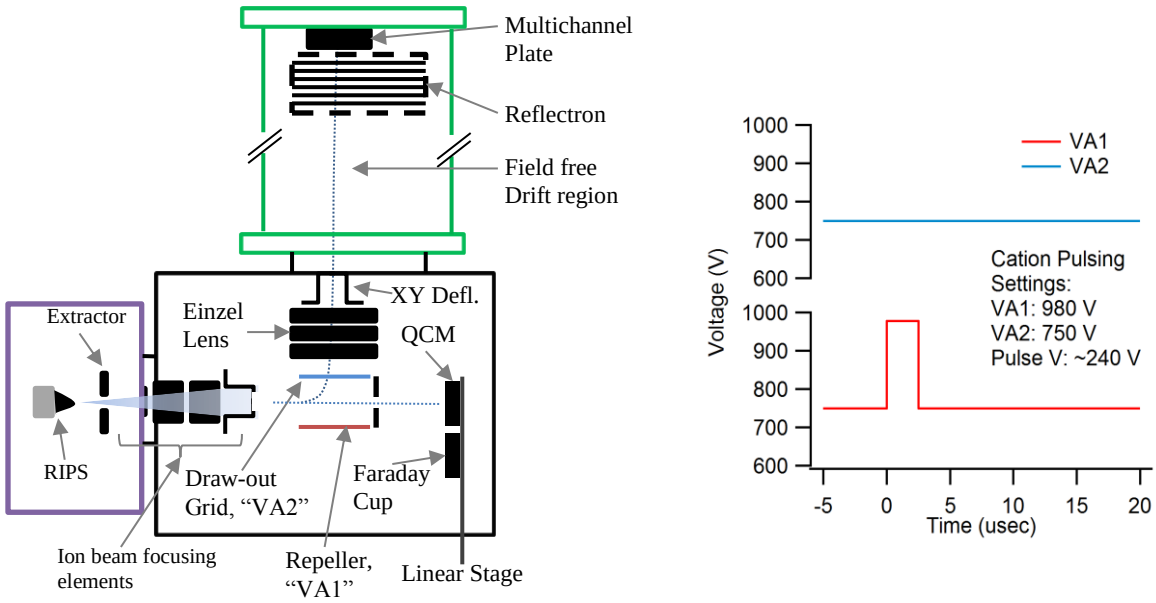

Figure 8. A schematic of the TOF facility illustrating the location of the RIPS located in the source chamber (purple outline) relative to the focusing elements, diagnostic instruments and TOF chamber (green). Also provided is the pulsing scheme for the TOF repeller (VA1) and Draw-out grid (VA2) while measuring cations.

Orthogonal extraction of the emitted ions into the TOF detection chamber was accomplished by first applying an equal voltage to both of the parallel extraction plates, referenced as VA1 and VA2 below. VA1 is termed the repeller plate and is opposite of VA2 on the detection axis. The base voltage applied to these plates acts as a high-pass kinetic energy filter for the emitted products. For example, if the plates are held at +750 V for cation emission, only cations with kinetic energies greater than 750 eV will enter the pulsing region. To redirect these ions orthogonally, a pulse is introduced to VA1. This square pulse was typically 2.5 µs long and 240 V in magnitude. With this pulsing scheme, the voltage on VA1 spends the vast majority of the time at the base voltage and similar to VA2; during the 2.5 µs period when it is active, VA1 is increased by 240 V resulting in deflection of ions onto the TOF detection axis, see Figure 8. Once ions are introduced to the TOF axis, an Einzel lens and an x-y deflector allow small

corrections to the alignment. Cations were detected by an MCP with a first stage voltage of -2000 V. Anion linear TOF spectra were not collected in these experiments but would require +3900 V split between the stages of the MCP. The generated signal was directed into two amplification stages using a 350 MHz Stanford Research pre-amplifier and then read by a multichannel scaler or a TOF card to produce TOF spectra.

Quadrupole mass spectra were collected for an electrospray from a RIPS using the following procedure. The preparation procedure was the same as the linear TOF experiments. Following the preparation, the apparatus was placed in the source chamber of quadrupole mass spectrometer. A 0.5-Hz square wave with constant amplitude of ±500 V was applied to the reservoir; a second 0.5-Hz square wave with varying peak-to-peak amplitude was applied to the extractor plate. The two square waves were 180 degrees out of phase. A Faraday cup was used to verify stable emission. The quadrupole RF signals were balanced once the source was in stable operation by maximizing the signal collected by the channeltron. A deflector, held at +/- 500 V for cations and anions, respectively, was biased to pulse the source ions into the channeltron. The front plate of the channeltron was biased to -2500 V for cations and +1800 V for anions while the back end of the channeltron was held at ground for cations and +4300 V for anions.

V. Results

A. Electrospray from the Rosensweig Instability Peak Source

Results of the electrospray experiments using the RIPS include the both mass spectra and QCM measurements for three different magnetic field strengths. Cation and anion TOF mass spectra of the electrospray beam were also collected for two ranges of emission current.

i. Characteristics of a Rosensweig Instability Peak Source

The RIPS was observed to have three stable modes of electrospray emission; one that was transient (designated ‘transient-emission’ in later sections), which began at the start of each emission test (start refers to either the first run with new ILFF in reservoir or a change between DC and AC operation) and would last for approximately five minutes, and two at which an electrospray could be emitted continuously, (designated ‘continuous-emission’ in later sections). The transient-emission mode would operate with an emission current range of 20-30 μA until it transitioned to either of the two continuous-emission modes. The two continuous-emission modes are termed the low-current mode and high-current mode, based on their respective operating emission currents of 1-10 μA and 30-80 μA. To move between the two continuous-emission modes, 50-100 V was either applied or removed from the extraction voltage. A fourth, unstable, mode also existed if the RIPS was operated at emission current greater than 100 μA, thus it was termed the very-high-current-mode. This mode was avoided during operation as it would lead to exceedingly long filamentary jets from the ILFF that bridged the gap between reservoir and extractor plate, shorting the emission. However, it did prove to be a mode in which high mass accumulation rates existed.

The continuous-emission modes were documented in the emission tests in the UHV chamber. The transition between the low-current and high-current modes was seen in the collected current (Figure 9) and also observed visually using the optical microscope (Figure 10).

The arrows between the orange and pink dashed lines in Figure 9 represent the transition between Figure 10 (a) (lower currents) and Figure 10 (b) (higher currents). Figure 10 also illustrates that the transition in between low- and high-current modes is associated with a change in the general shape of the Rosensweig peak, as well as a change in the apex of the peak, illustrated by inset images of Figure 10 (a) and (b).

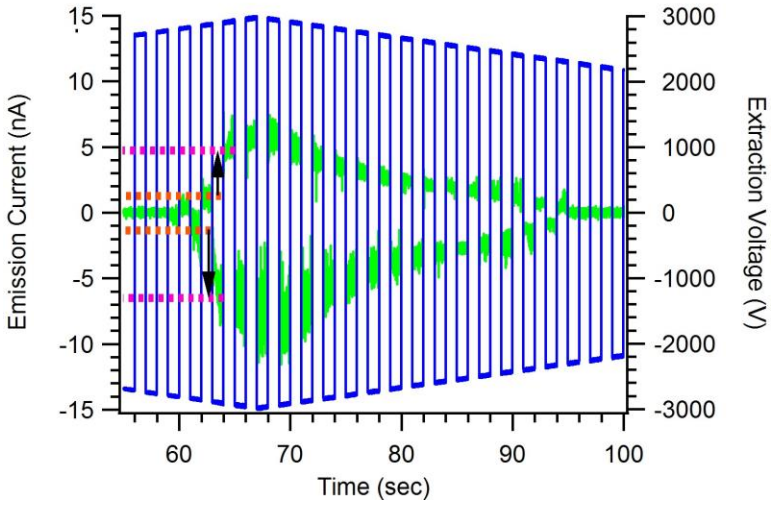

Figure 9. Telemetry of ILFF electrospray from Rosensweig instability source under 333.9 Gauss. The dashed lines show the transition of from low-current mode (orange lines at 1.2 nA and -1.3 nA) to high-current mode (pink lines at 4.7 nA and -6.5 nA) through an increase of |50 V| in extraction voltage.

Throughout emission testing of the RIPS mass flow measurements were collected using the QCM. Current measurements were also recorded using the Faraday cup, which had an aperture which limited the area of current collection to be equal with the QCM crystal area. The results are included in Table 1. It was observed that the mass accumulation rates were highest during the transient-emission current mode and the unstable, very-high-current mode, where they were an average of 5 ng/s. In the transient-emission mode, this mass accumulation rate continued for the entire five-minute period, after which time it dropped several orders of magnitude (see Table 1). In the very-high-current mode, however, the mass accumulation rate could only be maintained for approximately 30 seconds as longer times in this mode would induce the long filamentary jets that would bridge the extractor gap. It was also observed that a change between high- and low-current modes had only a small effect on the mass accumulation rate.

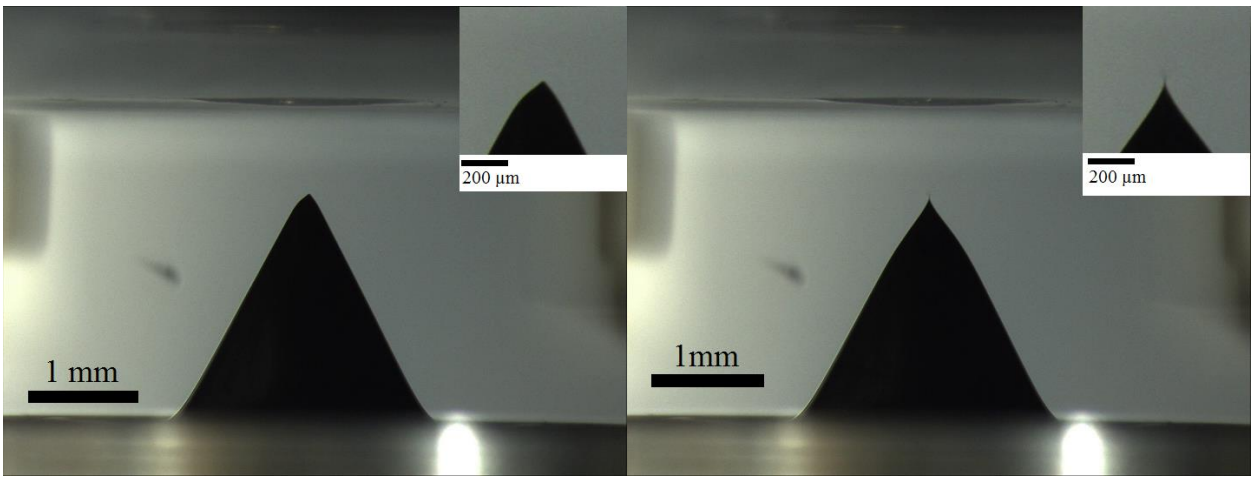

(a) **(b)**

Figure 10. Images capturing the operation of an ILFF electrospray emitted from a RIPS in the (a) low-current mode of operation, and (b) high-current mode of operation.

Table 1. Mass accumulation rates and current measurements collected throughout testing.

Emission Mode		Emission Current Range (μA)	B-Field (Gauss)	Average mass accumulation (ng/s)	Average Current Density (μA/mm^2)	All B-Fields		
						Average mass accumulation (ng/s)	Average Current Density (μA/mm^2)	Average m/q (amu/e)
Transient-Emission		20-30	333.9	5.388	1.415	**4.875**	**1.238**	**1.3E+05**
			520.5	6.415	2.122			
			690.5	2.821	0.177			
Continuous-Emission	Low-Current	1-10	333.9	0.014	0.062	**0.027**	**0.065**	**1.4E+04**
			520.5	0.009	0.035			
			690.5	0.058	0.097			
	High-Current	30-80	333.9	0.524	0.897	**0.334**	**0.680**	**1.7E+04**
			690.5	0.145	0.463			
Very-High-Current		>100	690.5	5.645	1.857	**5.645**	**1.857**	**1.0E+05**

ii. Cation Linear TOF Spectrum

The cation linear TOF spectrum for the RIPS was taken with 978 V, 750 V, and 240 V for VA1, VA2, and the pulsing voltage, respectively at magnetic field strengths of 333.9 and 520.5 Gauss. The resulting TOF mass spectra (Figure 11) contain only those ions with a kinetic energy within 50 eV/q of the emitter bias. Slower moving ions and droplets would be unable to overcome the barrier established by the +750 V potential established on VA1 and VA2 and subsequently cannot enter the pulsing region.

The spectra provided in Figure 12 (a) illustrates that no peaks or distributions were measured for m/q greater than 1000 amu/e. Figure 12 (b) focuses on the lower mass range where several mass peaks are apparent. The species at m/q = 111 amu is the parent $EMIM^+$ cation, referred to here as the n = 0 cation. The species at m/q = 502 amu is the $EMIM^+$ cation paired with a single neutral pair (i.e. $[EMIM][NTf_2]$ $EMIM^+$), commonly referred to as the n = 1 cation, where n indicates the number of neutral pairs bound to the ion.

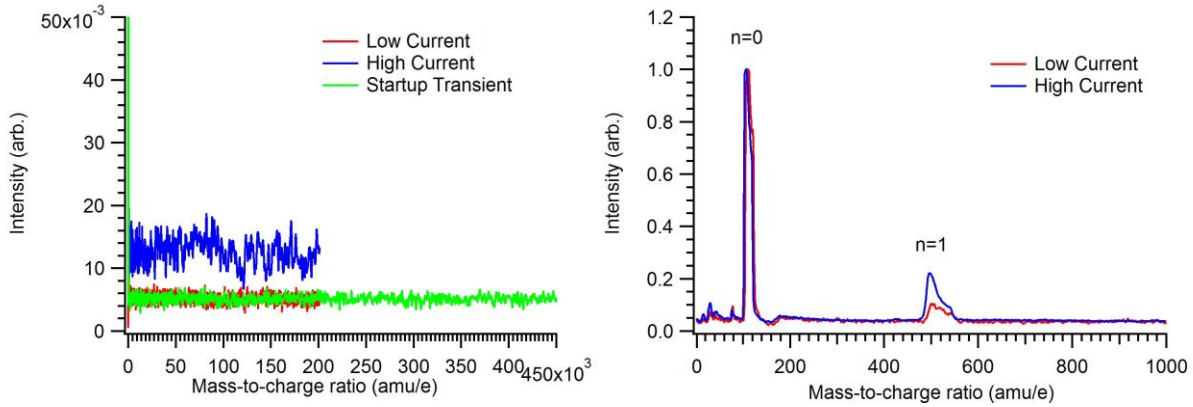

(a) **(b)**

Figure 11. (a) Full cation TOF mass spectra of an ILFF electrospray beam emitted from a single Rosensweig peak in low-current, high-current, and startup-transient emission modes. (b) Low mass range of the cation TOF mass spectra for low- and high-emission current modes. The magnetic field strength is 520.5 Gauss and the intensities are normalized such that the peaks at 111 amu are unity.

Also identified in the linear TOF mass spectrum in Figure 11 were peaks at m/q below 100 amu/e, which were present in both low- and high-current emission modes. The peak locations for these lighter masses were at m/q values of 15, 29, 42, 56, 83 and 96 amu/e. Figure 12 examines these lighter peaks as they were observed in the pure

IL electrospray TOF mass spectrum from the needle source. The inset of Figure 12 (a) magnifies the vertical range by a factor of 13.6. No masses above m/q = 502 were observed out to the maximum range of these particular scans (m/q = 12,000 for the IL spectrum and m/q = 22,000 for the ILFF spectrum).

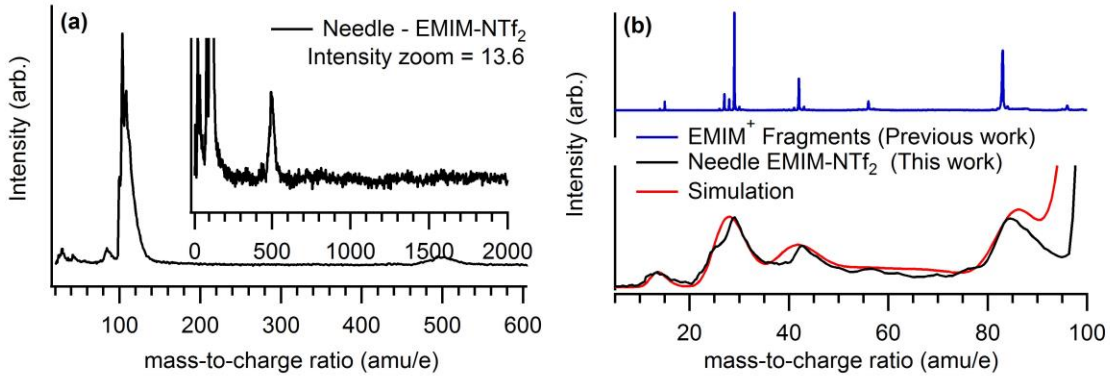

Figure 12. (a) Needle TOF mass spectrum using EMIM-NTf_2. (b) High resolution fragmentation of $EMIM^+$ (top), zoom of TOF spectra in (a) for less than 100 amu/e showing the measured spectra is consistent with molecular ions having 120 to 240 eV energy spread (red 'Simulation' curve).

The mass range below 100 amu/e is highlighted in Figure 12 (b) which includes the lower trace in Figure 12 (a) as well as previously measured pure EMIM-NTf_2 (no magnetic nanoparticles) high-resolution needle data, where fragment species were carefully and exclusively optimized. The high-resolution data in the top trace indicate the species are: 15 amu/e, assigned to CH_3^+; 29 amu/e, assigned to $C_2H_5^+$; 42 amu/e, assigned to $C_2NH_4^+$; 56 amu/e, assigned to $C_2N_2H_2^+$; 83 amu/e, assigned to MIM^+; and 96 amu/e, assigned to EIM^+. The fragmentation of cation species also generates some number of neutral species, for example, the fragmentation of $EMIM^+$ into a CH_3^+ ion will necessarily create an EIM (ethyl imidazolium) neutral fragment, which may or may not be picked up by a cation. The agreement between the previous high-resolution data and the current measurements suggest these assignments are applicable to the more general lens conditions used in these experiments.

Figure 12 (b) highlights an important feature in the recorded TOF mass spectra: the individual "lines" of the present data are significantly broader than might be expected from molecular ions. The line-widths of these peaks, and those that follow in subsequent sections, are a convolution of the bin size used in the detection system, the natural isotopic abundances of each atomic constituent in a species, and most importantly, a consequence of the true kinetic energy spread of a specific species. Typical electrospray systems studied for use in space propulsion applications have energy distributions of tens to hundreds of eV full-width half-maximum (FWHM) when interrogated using ion specific retarding potential analyses.[11,12] As these ions enter the pulsing region, ions with kinetic energies below the base VA1/VA2 potential (the V = 750 V potential in the pulse schematic of Figure 8) are rejected while those above the threshold are admitted into the pulsing region and retarded in the beam-axis direction. These admitted ions will have remaining axial kinetic energies in the 0-50 eV/q range depending on their respective pre-pulsing region kinetic energies. Once in the pulsing region, the position of the ions relative to the repeller plate (VA1) can significantly impact the velocity, and consequently, the line-width of the mass spectra in the TOF data.

Two-dimensional SIMION[27] simulations were performed with a set of electrodes generated to reproduce the pulsing region of the TOF mass spectrometer as shown in Figure 8. This region consisted of two 76.2-mm-long plates with an aperture of 6 mm located in the center of VA2. The two plates were separated from one another by 76.2 mm. VA1 was held at +978 V while VA2 was assigned +750 V. A plate perpendicular to the beam-axis direction was placed after the repeller plates and held at the VA1 potential. Along the flight tube axis (orthogonal to beam axis), the extracted ions encounter an Einzel lens and deflector before entering a 1-m-long grounded tube acting as the TOF chamber. Ion distributions were placed at three locations along the beam axis: 0 mm, 20 mm, and 43 mm from the entrance to the pulsing region. At these three positions, multiple distances, ranging from 2 to 72 mm, from VA1 were examined. 2500 ions were flown at each condition. For each 2500-ion simulation at a given initial position, a single mass was assigned a single positive charge with a uniform kinetic energy distribution ranging from 0.03 to 50 eV (i.e. ~750eV –800 eV) along the beam-axis direction. The simulated ions had a cone distributed with a half angle of 30 degrees. This cone distribution simulates a small amount of transverse velocity that would be expected in the generally-broad, ion plume of electrospray thrusters. An annotated schematic of the SIMION potential array is provided in Figure 13.

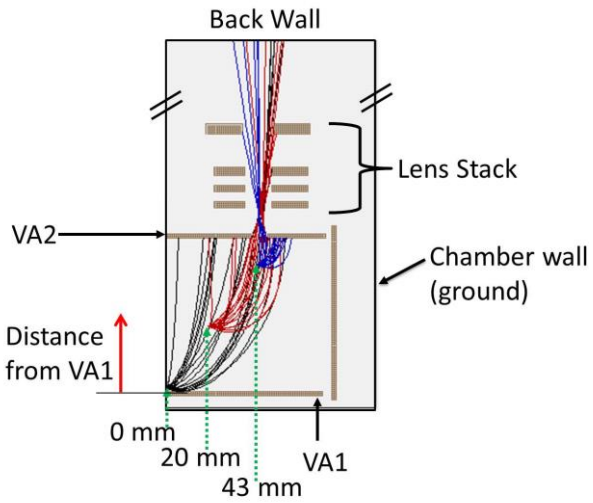

Figure 13. SIMION potential array with the three locations at which the 25000-ion cone distributions with m/q of 502 amu/e were generated.

The flight time, kinetic energy, and number of ions reaching the back wall located 1 m along the TOF axis were recorded for masses at 15, 111, 502, and 50,000 amu. The key findings are presented in Figure 14. In Figure 14 (a), the results from the m/q = 502 amu/e simulations are presented at two locations along the beam axis, at the entrance to the pulsing region (0 mm) and at the center of the pulsing region (43 mm). The x-axis encompasses points along the TOF axis measured relative to the VA1 position. In the top trace, the percentage of ions detected at the back wall to ions flown is presented. At 0 mm, ions could only be detected if they were within 40 mm (approximately halfway between VA1 and VA2) whereas the ions are detected at all distances when the ions are pulsed while in the center of the beam-axis within the pulsing region. However, at distances where ions are detected, the percentage of ions reaching the back wall of the TOF chamber is essentially similar at both positions along the beam axis. Nearly identical kinetic energies are observed for fixed distance from VA1 regardless of the position along the beam axis. Notably, the kinetic energy (KE) of the ions measured as they impact the wall ranges from 1010 eV to 761 eV over the entire distance from VA1 where ions have successfully transmitted along the TOF axis. The bottom trace of Figure 14 (a) presents the average flight time of the ions beginning at these locations. The standard deviation of the flight time taken from the 43-mm data is also presented. In contrast to the significant standard deviations observed in the flight time, the standard deviation of the average kinetic energy (not shown) was found to be typically 4-9 eV. The difference in flight time over 1 m for a 502 amu mass at 1000 eV and 800 eV is approximately 6 μs yet the average value found at near and far distances from VA1 appears to be contrary to what is expected from their respective kinetic energies. This discrepancy results from the different trajectories taken by the species that make it through the VA2 aperture. At distances close to VA1 (i.e. 2-22 mm), successfully extracted trajectories typically first move towards VA2 and then are repelled, whereas the ions at higher distance (greater than 22 mm from VA1) simply curve through the aperture, shortening their time spent in the pulsing acceleration region. In Figure 14 (b) the percent ion count and average kinetic energy as a function of the distance from VA1 are presented. The kinetic energy still exhibits a distance effect, as expected, and is independent of mass. The percentage of ions that reach the back wall is also found to be invariant of mass.

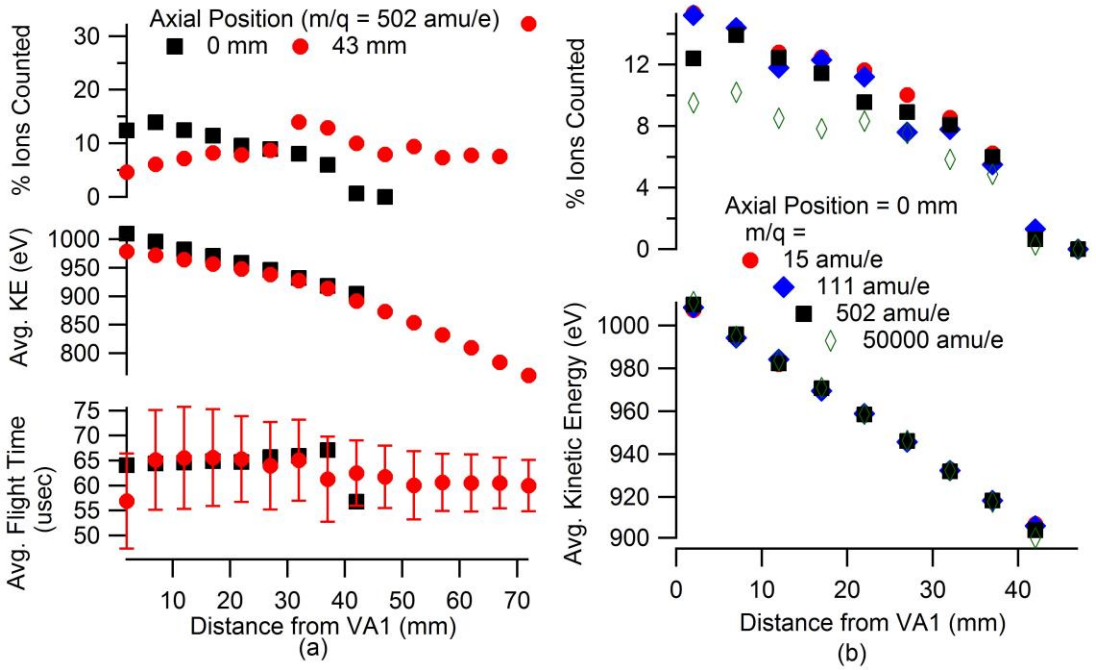

Figure 14. Results from SIMION simulation of the TOF pulsing region illustrating the percentage-of-ions that enter the flight chamber and average kinetic energy of ions versus (a) position in pulsing region and (b) m/q of the ions. Also in (a) average flight time of ions versus position in pulsing region (bottom).

Using the specific m/q values from the high-resolution data, their respective intensity ratios and the findings from the SIMION simulations, the needle TOF mass spectrum is simulated in the flight time domain and then converted to the mass domain and presented as the simulation trace in Figure 12 (b) All masses below 83 amu were modeled with kinetic energy line-widths equal to the pulsing potential (+240 eV) and centered at the VA1 voltage suggesting these species are detected at all positions in the pulsing region. As the mass increases the required kinetic energy line-width necessary to generate the proper mass and flight time line-widths becomes smaller and smaller, although the average kinetic energy appears to still be close to the value of VA1. The product of this simulation is a qualitatively accurate intensity versus time-of-flight mass spectrum.

iii. Cation Quadrupole Mass Spectrum

Quadrupole mass spectra were collected for the ILFF electrospray cation beam emitted from the RIPS under a magnetic field strength of 520.5 Gauss at the reservoir surface. The RIPS operated in both low-current and high-current modes during collection. The mass spectrum in Figure 15 (a) was collected during low-current emission mode and has peaks at m/q of 42, 83,111, 178, 435, and 502 amu/e. The 42 and 83 amu/e are identified as fragments of the $EMIM^+$ (n = 0) cation species described in section V-A ii. The 111 and 502 amu/e peaks are at known m/q, which represent the n = 0 cation species and [EMIM][NTf2] $EMIM^+$ (n = 1) cation species, respectively. The 178 amu/e peak is identified as the neutral fragment HMIM attached to an EIM^+ fragment. The 435 amu/e peak is unknown, but could be fragments of n = 0 cation attached to fragments of the n = 0 cation or ILFF polymer. The mass spectrum in Figure 15 (b) was collected during high-current emission mode and has peaks at the same m/q as observed in the low-current mass spectrum, as well as peaks at m/q of 124, 138, 147, and 571 amu/e. All of these peaks can be identified as m/q for fragments of the n = 0 cation attached to ion neutral fragments created by the fragmentation of the aforementioned cation species.

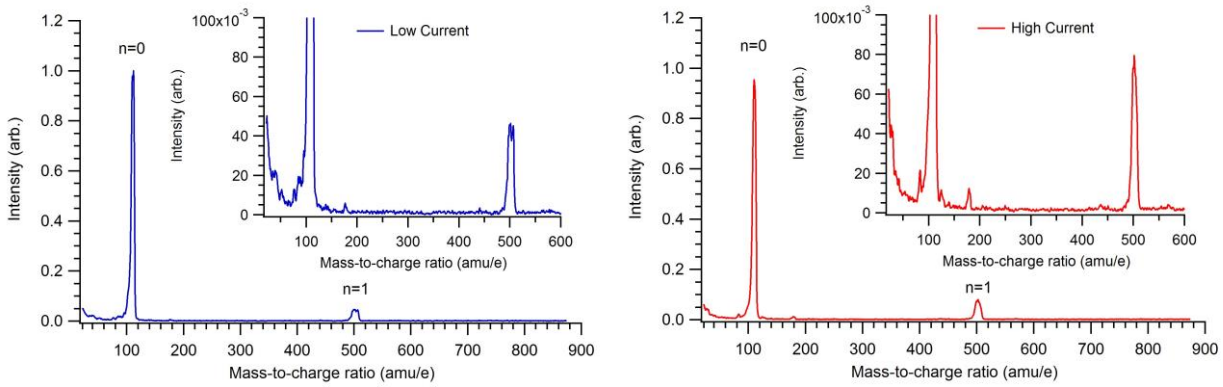

(a) **(b)**

Figure 15. Full and partial (inset focusing on the smaller peaks) cation quadrupole mass spectra of an ILFF electrospray beam emitted from a single Rosensweig peak during (a) low-current emission mode and (b) high-current emission mode. The intensities are normalized such that the peak at 111 amu/e is unity.

iv. Anion Quadrupole Mass Spectrum

Quadrupole mass spectra were collected for the ILFF electrospray anion beam emitted from the RIPS operating in both low- and high-current emission modes and under a magnetic field strength of 520.5 Gauss at the reservoir surface. The mass spectrum in Figure 16 (a) was collected during low-current emission mode and has peaks at m/q of 264, 280, and 671 amu/e. The 264 amu/e peak is unknown, whereas the 280 and 671 amu/e peaks are at known m/q which represent the $NTf2^-$ (n = 0) anion species and [EMIM][NTf2] $NTf2^-$ (n = 1) anion species, respectively. The mass spectrum in Figure 16 (b) was collected during high-current emission mode and has peaks at the same m/q as observed in the low-current mass spectrum, as well as peaks at m/q of 78, 147, 192, 215, 230, 308, 327, 607 and 740 amu/e. A majority of these peaks can be identified as m/q for fragments of the n = 0 anion, specifically NSO_2^-, $CF_3SO_2N^-$, $[NSO_2^-][CF_3SO_2N]$, $[CF_3SO_2N^-][CF_3]$, [NSO2-][CF3SO2NSO2CF], [EMIM][NTf2]$[CF_3SO_2N^-][CF_3]$, and [EMIM][NTf2] $NTf2^-$ $[CF_3]$ for the 78, 147, 215, 308, 607 and 740 amu/e peaks, respectively. The 229 and 327 amu/e peaks are unknown and could represent a fragment of the polymer attached to fragment of the n = 0 anion.

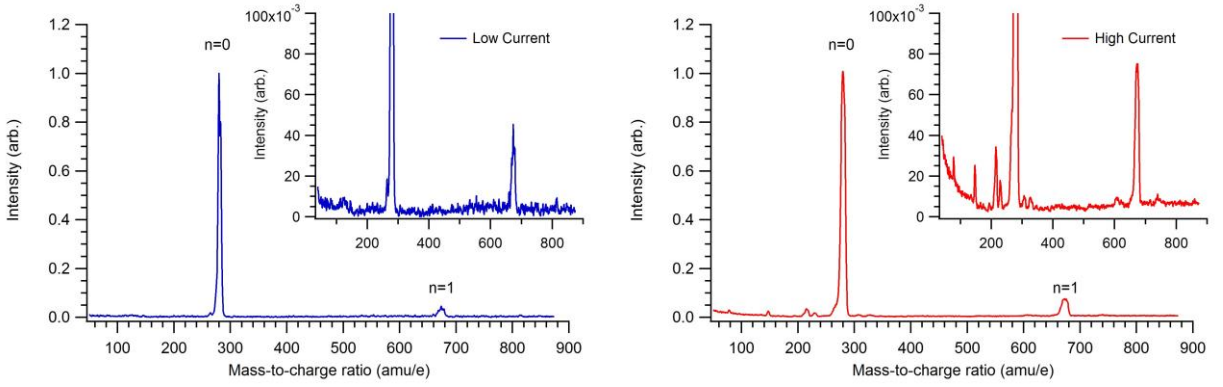

(a) **(b)**

Figure 16. Full and partial (inset focusing on the smaller peaks) anion quadrupole mass spectra of an ILFF electrospray beam emitted from a single Rosensweig peak during (a) low-current emission mode and (b) high-current emission mode. The intensities are normalized such that the peak at 280 amu/e is unity.

VI. Discussion

The results in Section V document the mass spectra of an ILFF electrospray beam from a RIPS. There are several observations made on the spectra and the operation of the ILFF electrospray that will be discussed in the following sections VI-A through VI-E.

A. Mass Flow Rate Variability

Past studies on the emission of ILFF from a Rosensweig instability peak have noted visual evidence of dark residue indicative of nanoparticles on the collector plate.[8] This residue accumulation could only arise from very high mass flow rates that include emission of nanoparticles. Previous literature relating to the study of ionic liquids and electrospray thruster research have determined that the existence of droplets in the electrospray beam is a consequence of high mass flow rates (7.5 ng/s) and large average m/q (25,000 amu/e) values.[12] It was assumed that the main fraction of the mass flow in these studies results from large charged-droplets. In the case of mixed ion-droplet operational mode, the average m/q value as measured by a current sensor and a mass sensor will necessarily be a weighted average between the m/q of the small ions and the true m/q value of the large droplets.

For the ILFF used in this research, the mass of a 25-nm-diameter nanoparticle with associated copolymer and a 22.5 nm thick layer of EMIM-NTf_2 (the hydrodynamic diameter of particles in similar ILFFs is approximately 70 nm[17]) would be 196,000 amu. Therefore, a droplet involving the nanoparticle and copolymer emitted from the RIPS would be in the m/q range of 350 to 196,000 amu/e (the lower limit is the Rayleigh limit of a 70-nm diameter IL and the upper limit is assuming the droplet is singly-charged). The average m/q value presented in Table 1 does indicate that significant m/q values were observed for the very-high-current and transient-emission modes. Since small ionic species were also observed in the TOF mass spectrum in these operational modes, the average m/q is weighted by some factor towards a smaller m/q value. Unfortunately, droplets could not be definitively identified in the TOF mass spectrum. During the transient-emission and very-high-current modes of operation, the average m/q, as measured by the Faraday cup and QCM, ranged from 100,000 to 130,000 amu/e. Over a period of approximately five minutes operating in transient-emission or very-high-current modes, the average m/q fell to a value near 15,000 amu/e. This transition to smaller masses indicates that droplet emission ceased, ion production greatly increased, or some lesser combination of the two. Time-of-flight mass spectra taken at early operational times qualitatively reproduced those taken at low m/q value periods in terms of species identities and relative intensities. Qualitatively, this observation suggests that small ion production did not greatly increase and instead droplet formation decreased.

B. Large Mass and Droplet Presence

Average m/q measurements collected of the ILFF electrospray are much greater than the mass of the largest cation or anion species observed, 502 amu/e and 671 amu/e, respectively, which would suggest the presence of large masses or droplets during emission. However, when examining the full linear TOF mass spectrum for the cation electrospray beam during low- current, high-current, and the startup transient emission modes (Figure 11) no distributions or peaks exist in range of m/q greater than 1000 amu/e. This observation is disconcerting for the startup transient emission mode which had a measured average m/q of 100,000 amu/e; this suggests that some indication of large masses should be present in the mass spectrum.

A possibility for the absence of these larger masses is that their net charge is zero. This would mean that these masses were not pulsed orthogonally into the TOF chamber for collection. Another possibility is that the TOF instrument is not suitable for droplet collection, especially if the emitted droplets have a wide, non-Gaussian distribution of masses.

C. Varying Emission Current

The magnitude of the emission current had a large effect on the TOF and quadrupole mass spectra in both polarities of emission. Figure 17 shows the comparison between the mass spectra of electrosprays collected during low-current and high-current emission modes. The emission current comparisons for both anion and cation electrosprays provide evidence that a correlation exist between the emitted current and the ratio of the relative intensities of n = 0 peak to any other peak; e.g. the ratio of relative intensity between the n = 0 peak and n = 1 peak decreases with the increase in emission current. A similar observation of this correlation was seen in the cation linear TOF mass spectra provided in Figure 11 (b). Furthermore, multiple peaks with m/q corresponding to ion fragments, as identified in section V-A. iii. and iv., appear in the cation and anion quadrupole mass spectra collected during high-current emission mode. This provides further evidence of a correlation between the magnitude of emission current and the mass spectra.

The correlation could be attributed to a change in enhancement of the electric field caused by the changing shape of the Rosensweig instability peak. Prior electrospray testing using the Rosensweig instability has shown that when emitting in the low-current mode the apex and foundation of the peak has noticeably different geometry than when in the high-current mode (Figure 10). This change in geometry would affect the electric field used to extract the electrospray beam. This has been observed in literature reporting data from capillary emitters which revealed a proportionality between the cation species ratio and electric field.[28] A change in the electric field caused by the

change in geometry of the Rosensweig peak would therefore account for the increase in the n = 1 cation species peak with respect to n = 0 cation species and the appearance of ion fragments as the emission current increases.

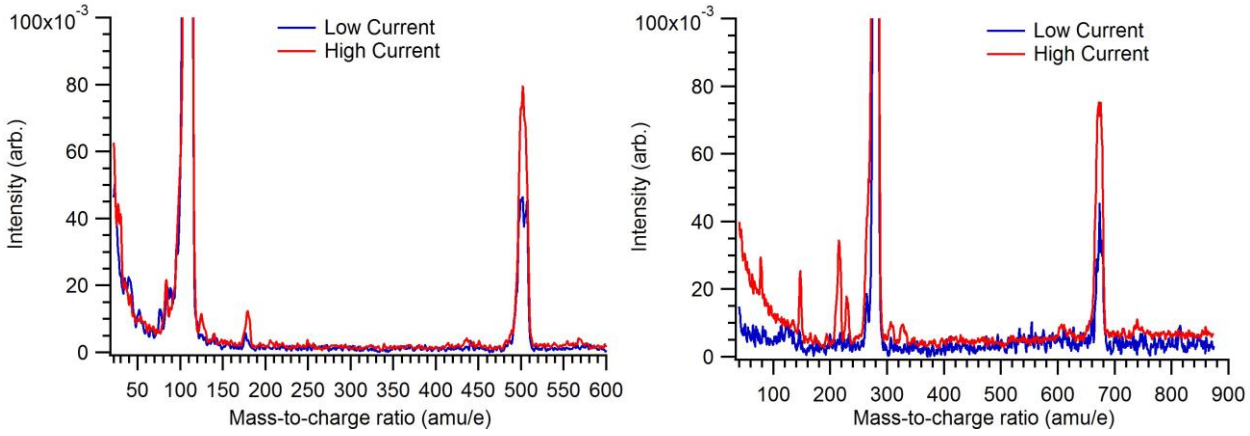

Figure 17. Quadrupole mass spectra of (a) a cation electrospray from the RIPS operating in low- and high-current modes, and (b) an anion electrospray from the RIPS operating in low- and high-current modes. Both are under a magnetic field strength of 520.5 Gauss. Intensities are normalized such that the peak at (a) 111 amu/e or (b) 280 amu/e is unity.

D. Varying Magnetic Field Strength

Magnetic field strength appeared to have little effect on the mass spectra of the RIPS electrospray. Figure 18 shows the cation TOF cation mass spectra of the RIPS operating with applied magnetic field strengths of 333.9 and 520.5 Gauss. From these curves there appears to be no change in the emitted masses or the relative intensities of these masses. Furthermore, the mass accumulation measurements show no correlation to the a change in magnetic field strength. However, the change in magnetic field strength was observed to change the overall shape of the Rosensweig instability peak. Similar changes in the peak shape had an effect on electrospray beam when emission current was the catalyst for the shape change; this may suggest that an correlation between the magnetic field strength and the mass spectra of the electrospray beam exists but is yet to be measured or observed.

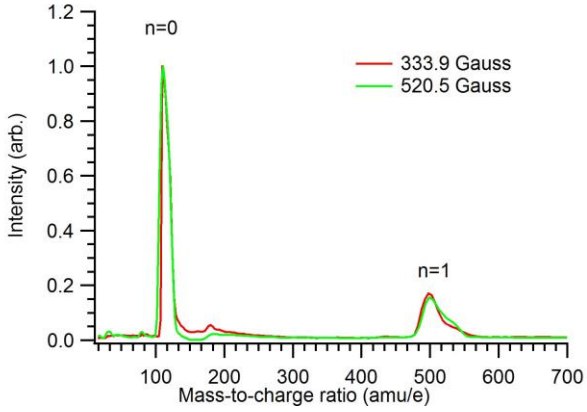

Figure 18. Linear TOF mass spectra of the RIPS cation electrospray operating in high-current mode and under two magnetic field strengths. Intensities are normalized such that the peak at 111 amu/e is unity.

E. Rosensweig Instability Peak Source vs. Needle Emitter Source

A comparison between the quadrupole mass spectra of the ILFF electrospray from a RIPS and quadrupole mass spectra acquire in a previous study using a pure IL electrospray solid needle emitter source[29] is useful to reference the new RIPS technique against an established device. It also provides an opportunity to determine if any components of the ILFF contribute to the ionic species. Figure 19 shows the cation and anion mass spectra of electrosprays from both the needle source and RIPS. Evidence of unusual ionic species compared to the needle source occurs in both the cation TOF mass spectra, and the anion and cation quadrupole mass spectra is seen for masses between the n = 0 and n = 1 peaks. As noted in section V-A. iii. and iv. many of these unusual ionic species can be identified as fragments of the n = 0 ions, or ion fragments attached to neutral fragments. For several peaks, specifically the 435 amu/e peak in the cation spectrum and the 230 and 327 amu/e peaks in the anion spectrum, no m/q that included some combination of the respective ion and its fragments could be assigned. Therefore it was believed that some combination of the respective ion, its fragments, and fragments of the polymer described in section III-A. Some possible fragments from the polymer include a single PDA block, the associated $CH_3CHCOOH$ end group, and COOH, a fragment of the end group. Using these polymer fragments, assignments for the unknown peaks were made. The unknown cation peak was identified as a single PDA block and the associated $CH_3CHCOOH$ end group attached to the n = 0 cation, which would produce a peak at 432 amu/e; this within the error of the peak-width. The unknown anion peaks were identified as a single PDA block attached to an n = 0 anion, and a COOH fragment attached to an n = 0 anion, which produce peaks at 230 amu/e and 325 amu/e, respectively. Both assigned m/q are within the error of the peak-width.

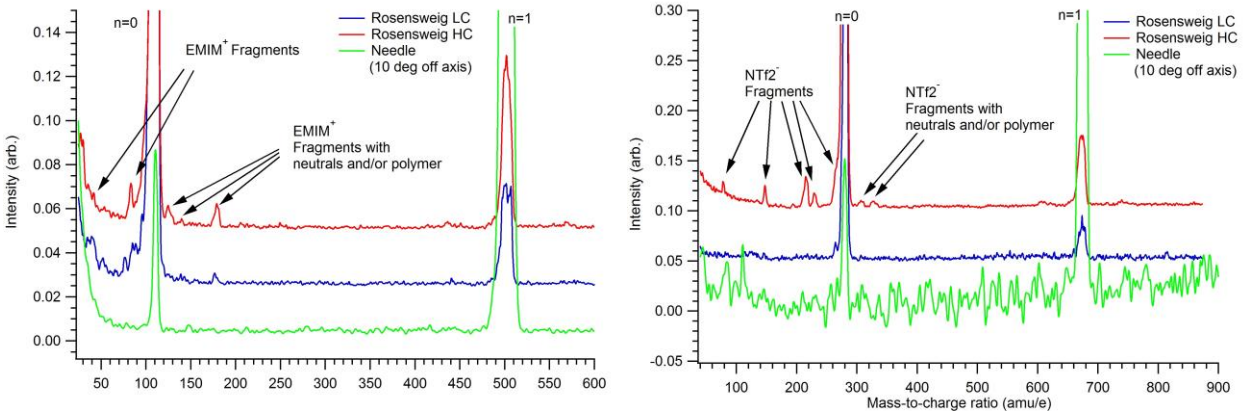

(a) **(b)**

Figure 19. (a) Cation and (b) anion TOF mass spectra of an electrospray beam from the RIPS and the needle emitter source. Note the baselines are intentionally offset for clarity. The magnetic field strength for the RIPS was 520.5 Gauss.

The cation and anion spectra of the needle source show many similarities to the cation and anion spectra of the RIPS operating in low-current emission mode; suggesting that the RIPS operates similarly to a needle source for that specific emission mode. When in high-current mode, though, the RIPS emitted several peaks that are not seen in the needle spectrum. This would lead to a significant difference in the specific impulse and thrust of the RIPS when compared to the needle source.

The emission current of the two sources differed as well. The needle source operated stably at 1.75±0.1 μA for the entire hour span of testing. The RIPS had three emission modes, two of which, the low- and high-current modes, can be sustained continuously, however, not as stably with emission currents of 5±4.5 μA and 50±25 μA. The third transient-emission mode lasted only five minutes, though its emission current varied relatively less at 25±4.5 μA.

VII. Conclusion

An electrospray apparatus which used an ILFF propellant and emitter formed through the Rosensweig instability as the emission site was built, and its beam composition was measured using a QCM, a quadrupole mass spectrometer, and a TOF mass spectrometer. The ILFF used was comprised of 27 wt% iron-oxide nanoparticles, 4.5 wt% copolymer, and 68.5 wt% EMIM-NTf_2. The apparatus used one, two, or three permanent magnets to instigate the Rosensweig instability which produced magnetic field strengths that ranged from 333.9 Gauss to 690.5 Gauss. The mass spectra collected are the first to measure of the composition of an ILFF electrospray beam emitted over

two magnetic field strengths from a RIPS. During emission of the ILFF three stable modes of operation were observed, a transient mode at the start of testing which emitted at 20-30 μA, a second at low currents of 1-10 μA, and a third at higher currents of 30-80 μA, which were called transient-emission, low-current, and high-current modes, respectively. It was also discovered that the RIPS would emit with a high mass flow rate, up to 6 ng/s, in the first minutes of emission, after which the its flow rate dropped several orders of magnitude during sustained operation.

Large masses and droplets were absent in the linear TOF mass spectrum despite the large average m/q measured using the QCM and Faraday cup. This is believed to be the consequence of a net-zero charge of the emitted droplets, which inhibits the TOF repeller plate in turning these particles into the TOF chamber for collection and measurement. Another possibility is that the TOF mass spectrometer was not capable of measuring the emitted droplets which may span a wide range of m/q.

Analyzing the collected linear TOF and quadrupole mass spectra revealed that the electrospray beams of the low- and high-current emission modes differed in the ratio of $EMIM^+$ ions to $[EMIM][NTf_2]$ $EMIM^+$ ions; specifically the spectra displayed a correlation between emission current and the relative intensity fraction of the $[EMIM][NTf_2]$ $EMIM^+$ ion species. Furthermore, the electrospray beams from the high-current emission mode were shown to be partially-comprised of fragments of the respectively anion or cation. This correlation is believed to be a consequence of change in shape of the Rosensweig peak during adjustments in extraction voltage.

Through a comparison between the quadrupole mass spectra from the RIPS to the quadrupole mass spectra from a needle source it was discovered that multiple peaks appear in both cation and anion mass spectra that do not appear in the pure IL cation or anion spectra. The peaks in the cation spectrum are believed to be associated with different combinations of the fragmented n = 0 cation, with a single peak identified as a combination of one fragment group of the polymer and the n = 0 cation. The peaks in the anion spectrum are believed to be associated with fragments of the n = 0 anion, with two peaks associated with fragments of the polymer paired with the n = 0 anion, and a fragment of the n = 0 anion.

An adjustment in the magnetic field strength was shown to change the shape of the Rosensweig peak. However, there appeared to be no correlation between the H-field and the cation or anion spectra.

Acknowledgments

The authors would like to thank members of the Michigan Tech's Isp Lab for all the thought-provoking discussions, specifically Edmond Meyer and Brandon Jackson for helping design the RIPS, and Mark Hopkins for showing us the wonders of ferrofluids and for teaching the ways of LabView data acquisition. Also they would like to thank Marty Toth and Jesse Nordeng for machining all custom components for the experiments. The authors would also like to thank the Air Force Research Lab for providing the facilities to conduct the testing. They would also like to thank the US Air Force Office of Scientific Research: International AOARD and Sirtex Medical Limited for funding the development of the ILFFs, and Steve Jones and Stephanie Bickley for designing and preparing the monodomain magnetic particles. The material is based upon work supported by NASA under award No NNX13AM73H. Any opinions, findings, and conclusions or recommendations expressed in this material are those of the authors and do not necessarily reflect the views of the National Aeronautics and Space Administration.

References

1. Rosensweig, R.E., "Magnetic Fluids," Annual Review of Fluid Mechanics, 19, 1987, pp. 437-461
2. Odenbach, S., "Ferrofluids—magnetically controlled suspensions," Colloids and Surfaces A: Physicochemical and Engineering Aspects, 217, 2003, pp. 171-178
3. Raj, K., B. Moskowitz, and R. Casciari, "Advances in ferrofluid technology," Journal of Magnetism and Magnetic Materials, 149, 1995, pp. 174-180
4. Laurent, S., et al., "Magnetic iron oxide nanoparticles: synthesis, stabilization, vectorization, physicochemical characterizations, and biological applications," Chemical reviews, 108, 2008, pp. 2064-2110
5. Halbreich, A., et al., "Biomedical applications of maghemite ferrofluid," Biochimie, 80, 1998, pp. 379-390
6. Rudolf, H., et al., "Magnetic particle hyperthermia: nanoparticle magnetism and materials development for cancer therapy," Journal of Physics: Condensed Matter, 18, 2006, pp. S2919
7. Meyer, E.J., Lyon B. King, "Electrospray from an Ionic Liquid Ferrofluid utilizing the Rosensweig Instability " *49th AIAA/ASME/SAE/ASEE Joint Propulsion Conference & Exhibit,* San Jose, CA, 14-17 July 2013
8. Meyer, E.J., Lyon B. King, Nirmesh Jain, and Brian S. Hawkett, " Ionic liquid ferrofluid electrospray with EMIM-NTf2 and ferrofluid mode studies with FerroTec EFH-1 in a non-uniform magnetic field " *33rd International Electric Propulsion Conference* The George Washington University, USA, 6 -10 October 2013
9. Boudouvis, A.G., et al., "Normal field instability and patterns in pools of ferrofluid," Journal of Magnetism and Magnetic Materials, 65, 1987, pp. 307-310
10. Chiu, Y.-H., et al., "Mass Spectrometric Analysis of Ion Emission for Selected Colloid Thruster Fuels," *39th AIAA/ASME/SAE/ASEE Joint Propulsion Conference and Exhibit*,
11. Chiu, Y.-H., et al., "Mass Spectrometric Analysis of Colloid Thruster Ion Emission from Selected Propellants," Journal of Propulsion and Power, 21, 2005, pp. 416-423
12. Chiu, Y.H., et al., "Vacuum electrospray ionization study of the ionic liquid, [Emim][Im]," International Journal of Mass Spectrometry, 265, 2007, pp. 146-158
13. Prince, B.D., B.A. Fritz, and Y.-H. Chiu, *Ionic Liquids in Electrospray Propulsion Systems*, in *Ionic Liquids: Science and Applications*2012, American Chemical Society. p. 27-49.
14. Lenguito, G., et al., "Multiplexed Electrospray for Space Propulsion Applications," *46th AIAA/ASME/SAE/ASEE Joint Propulsion Conference & Exhibit,* Nashville, TN, 24-28 July 2010
15. Lozano, P. and M. Martínez-Sánchez, "On the dynamic response of externally wetted ionic liquid ion sources," Journal of Physics D: Applied Physics, 38, 2005, pp. 2371
16. Jain, N., et al., "Optimized steric stabilization of aqueous ferrofluids and magnetic nanoparticles," Langmuir, 2009, pp.
17. Jain, N., et al., "Stable and Water-Tolerant Ionic Liquid Ferrofluids," ACS Applied Materials & Interfaces, 3, 2011, pp. 662-667
18. Rosensweig, R.E., *Ferrohydrodynamics* 1985, Mineola: Dover Publications, Inc.
19. Gamero-Castaño, M. and V. Hruby, "Electrospray as a Source of Nanoparticles for Efficient Colloid Thrusters," Journal of Propulsion and Power, 17, 2001, pp. 977-987
20. Miller, S.W., B.D. Prince, and J.L. Rovey, "Capillary Extraction of the Ionic Liquid [Bmim][DCA] for Variable Flow Rate Operations," *48th AIAA/ASME/SAE/ASEE Joint Propulsion Conference & Exhibit,* Atlanta, Georgia,
21. Miller, S.W., et al., "Electrospray of 1-Butyl-3-Methylimidazolium Dicyanamide Under Variable Flow Rate Operations," Journal of Propulsion and Power, 2014, pp. 1-10
22. Lozano, P.C., "Studies on the Ion-Droplet Mixed Regime in Colloid Thrusters," Department of Aeronautics and Astronautics, Massachusetts Institute of Technology, 2003
23. Romero-Sanz, I., et al., "Source of heavy molecular ions based on Taylor cones of ionic liquids operating in the pure ion evaporation regime," Journal of Applied Physics, 94, 2003, pp. 3599-3605
24. Gamero-Castaño, M., "The structure of electrospray beams in vacuum," Journal of Fluid Mechanics, 604, 2008, pp. 339-368
25. Gassend, B.L.P., "A Fully Microfabricated Two-Dimensional Electrospray Array with Applications to Space Propulsion," Department of Electrical Engineering and Computer Science, Massachusetts Institute of Technology, 2007
26. Krpoun, R. and H.R. Shea, "Integrated out-of-plane nanoelectrospray thruster arrays for spacecraft propulsion," Journal of Micromechanics and Microengineering, 19, 2009, pp. 045019
27. Dahl, D.A., "SIMION for the personal computer in reflection," International Journal of Mass Spectrometry, 200, 2000, pp.
28. Terhune, K.J., Lyon B. King, "Ion and Droplet Mass Measurements of an Electrospray Emitter using an ExB Filter," *32nd International Electric Propulsion Conference,* Wiesbaden, Germany, 11 - 15 September
29. Ticknor, B., et al., "Effect of Aspect Ratio on the Wettability and Electrospray Properties of Porous Tungsten Emitters with the Ionic Liquid [Emim][Im]," *46th AIAA/ASME/SAE/ASEE Joint Propulsion Conference & Exhibit,*